CrystEngComm

Dissecting Kinetic Pathways to Formation of the Fibrillar Objects in Molecular Gels Using Synchrotron FT-IR

SCHOLARONE™
Manuscripts

Dissecting Kinetic Pathways to Formation of the Fibrillar Objects in Molecular Gels Using Synchrotron FT-IR

Michael A. Rogers, [1] Xia Liu,[2] V. Ajay Mallia,[3] and Richard G.Weiss[3,4*]

Abstract

The processes associated with sol-to-molecular gel transitions are often difficult to follow in real time due to the characteristically short time-frames for pseudo-crystallization leading to fibrillar objects and establishment of their 3-dimensional networks. We use fast infrared spectroscopic methods to overcome these difficulties in a 'demonstration of principle' study: the nucleation and growth of crystallites of two amide derivatives of (R)-12-hydroxystearic acid, (R)-12-hydroxy-N-propyloctadecanamide (**1**) and (R)-12-hydroxyoctadecanamide (**2**), in mineral oil over a range of temperatures. First, the gel properties were established by optical microscopic, differential scanning calorimetric, and rheological measurements. Thereafter, the environments experienced by individual functional groups within **1** and **2** have been followed as a function of gelation time, and the data were treated by Avrami and fractal models in order to extract the kinetics, activation energies, and natures of the growth processes. The data both provide insights and raise new questions concerning the manner by which the amide and hydroxyl groups interact over the critical time periods during which the fibrillar networks of the gels are being established. The results demonstrate the utility of fast infrared spectroscopy as a valuable new tool to probe intimate details of the processes associated with self-assembly. The techniques and methodologies described are amenable to use with a wide range of gelating (or other aggregating) systems.

1) Department of Food Science, University of Guelph, Guelph, ON, N1G2W1, Canada
2) Mid-IR Beamline, Canadian Light Source, Saskatoon, SK, S7N2V3, Canada
3) Department of Chemistry, Georgetown University, Washington, DC 20057-1227, USA
4) Institute for Soft Matter Synthesis and Metrology, Georgetown University, Washington, DC 20057-1227, USA
* corresponding author: weiss@georgetown.edu

Introduction

Self-assembly, utilizing hierarchical aggregation of molecular components, is an appealing process for fabricating complex, supramolecular nanostructures that spontaneously generate ordered crystalline ensembles.[1] However, the mechanisms that direct self-assembly of many nanostructures, including those of molecular gels, are poorly understood compared to their higher-ordered crystalline counterparts.[2, 3] In part, the problem can be traced to the small sizes of the objects being formed and the lack of techniques capable of following the rapid rates at which the aggregating species develop. Research emphasis and technique development have traditionally focused on high-dimensionality crystals in fields such as oxide and phosphate inorganic chemistry,[5] polymer chemistry[6] and lipid chemistry. Low-dimensional crystal aggregates are at the forefront of research areas dealing with colloidal fat crystal chemistry,[7-9] ceramics,[4] and chemo-responsive gels.[5]

To advance these technologies will require a fundamental understanding of the individual steps associated with the aggregation, nucleation and crystal growth mechanisms leading to the eventual nano-scale objects.[6] Those steps for architectures established in molecular gels depend on several variables, including solvent properties/structures,[7-16] molecular gelator structures,[17, 18] thermodynamic driving forces,[19] and the kinetic pathways.[17, 20-27] Each of these plays an important role in mediating the aggregation of initially dissolved gelator molecules and their growth into nanoscale objects, usually fibers.[1, 3]

The vast majority of molecular gels spontaneously form self-assembled fibrillar networks (SAFiNs) via aggregation-nucleation-growth pathways upon cooling supersaturated solution/sol.[28] The thermodynamic driving force in the supersaturated state (often termed the supercooled or undercooled state) supplies the impetus for phase separation Supercooling under isothermal conditions is defined as $\tau = (T^* - T)/T^*$; T^* is the critical temperature where gelation begins and T ($< T^*$) is the temperature at which the sample is incubated.[29] Cooling below T^* initiates microscopic phase separation of the gelator via stochastic nucleation driven by enthalpic forces.[30] Depending on the supercooling experienced by the system during gelation, numerous significant modifications of the SAFiN network have been reported. The most commonly reported change is from a supramolecular fibrillar network to a highly branched 'spherulitic-like' network.[26, 29, 31-34] Following nucleation, crystal growth increases the number of gelator molecules accreted onto the network of forming rods, tubes, or sheets. This process of aggregation requires a meticulous balance between the contrasting parameters of solubility and those controlling epitaxial growth.[35]

Here, we employ a fast spectroscopic method, Fourier-transform infrared spectroscopy (FT-IR) from a synchrotron source, to examine the kinetics of self-assembly of the SAFiNs of (R)-12-hydroxy-N-propyloctadecanamide (**1**) and (R)-12-hydroxyoctadecanamide (**2**) (Scheme 1) in mineral oil. Both gelators have been reported to gel numerous solvents[36] and **1** has been reported to undergo a gel-gel transition in CCl₄.[37] We demonstrate here the utility of FT-IR to follow the kinetics of such assembly processes and, in some cases, to provide detailed information about the timing of selective group-group interactions.

Scheme 1

1: R = C₃H₇
2: R = H
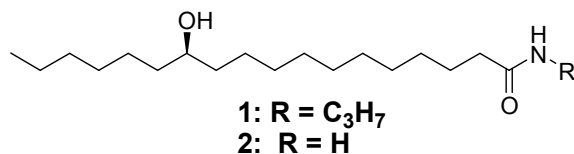
Results and Discussion

Demonstrations of gel character. The differential scanning calorimetry thermograms in Figures S1-S4 (Supporting Information figures are designated with an 'S' preceding the number.) confirm that 2 wt % mineral oil gels of both **1** and **2** exhibit a melting transition on heating and a crystallization transition on cooling that is reproducible in subsequent thermal cycles (Figure S2 and Figure S4); the transitions from the gel of **1** (Figure S1) are very weak, however. Regardless, the reproducibility demonstrates that the transitions are due to a change in the physical state

2

of the samples rather than chemical reaction. Our investigations with **1** and **2** in other liquids have demonstrated that these transitions are related to the crystallization (on cooling) or melting (on heating) of SAFiNs within the gel phases.[36] The temperatures of maximum heat flow on cooling—ca. 110 and 100 ºC for gels of **1** and **2**, respectively—are significantly higher than the incubation temperatures employed in the FT-IR kinetic studies; all of the experiments were conducted under supercooled conditions.

Furthermore, although the strain sweeps in Figure S5 and Figure S6 demonstrate that gels of both **1** and **2** are weak (N.B., they are no longer gels above ~1 and ~30 % strains, respectively), they are true gel because the values of *G'* and *G"* in frequency sweeps remain relatively constant, with *G' > G"*, throughout a very broad range of frequencies within their linear viscoelastic regions (Figure S7 and Figure S8).

FT-IR spectral studies. Spectroscopic methods, including FT-IR, have been employed previously to track aspects of the kinetics of self-assembly of molecular gels.[17, 23, 25, 28, 38-41] In doing so, it must be assumed that the phase volume of the new state or phase is proportional to the change in the signal intensity or peak position, depending on the mode of data acquisition; care must be taken to ensure that the changes in FT-IR signal intensity are not a result of changing temperature, but to changes associated with the environments of the gelator molecules as the gel is being formed. For this reason, the baseline values for these spectra were obtained from the sol states at the initiation of the experiments; thus, relative changes in signal intensity are being monitored.

A spectral feature of **1** and **2** in mineral oil at 1375 cm^{-1}, corresponding to aliphatic CH_3 stretching, is an example of a spectral feature that did not change as a function of aggregation when sols were incubated at temperatures below T* (Figures 1 and S9).[42] From plots of the peak areas as a function of incubation time, it is clear that the signal intensity changed as a linear function of the decreasing temperature until the final temperature was reached. Thereafter, no further change in signal intensity was discernible. Evidence that the SAFiNs of these gels had not formed prior to reaching the incubation temperatures is found in the comportment of the signal intensities of other IR bands.

Another indication that the increasing signal intensity is not a function of the self-assembly process governing SAFiN formation is the lack of a sigmoidal evolution of the new crystalline phase.[43-45] Such curves have been reported in the gelation of several other systems in which various analytical techniques were used to monitor the changes. The data from many of these can be fitted to the Avrami model (eq. 1):[19, 28, 43-46]

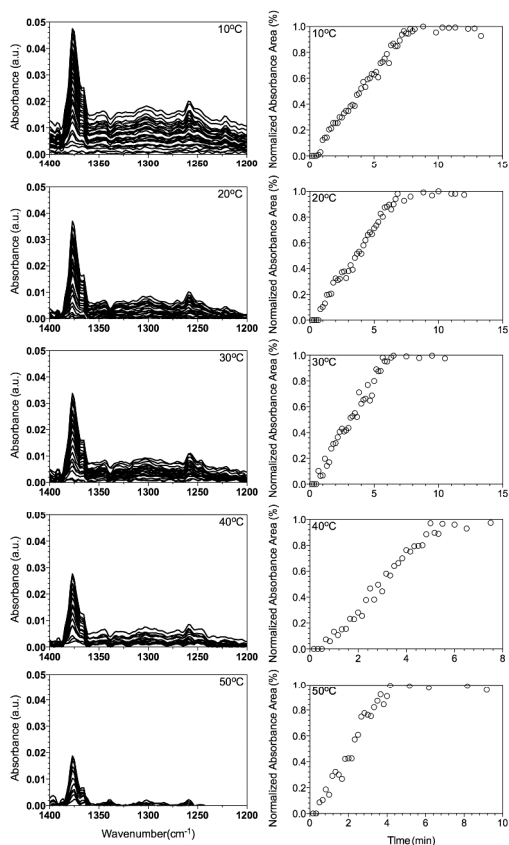$$\frac{Y}{Y_{max}} = 1 - e^{-K(x)^n} \tag{1}$$

Figure 1. Vertically offset FT-IR spectra for the aliphatic CH_3 stretch, using the sol spectra as the baseline, for formation of 2 wt % mineral oil gels of **1** at different temperatures (left). The peak areas at 1375 cm^{-1} were integrated and normalized by dividing the values by the maximum absorbance area obtained after holding the gel for 5 min at the crystallization temperature (right).

In eq, 1, Y/Y_{max} is the phase volume (i.e., the area under a particular peak), K is a rate constant whose units depend on the value of n, x is time, and n is the Avrami exponent. The two Avrami parameters of importance are the exponent, n, and the rate constant, K. The Avrami exponent is a unitless measure of the mode of nucleation, either being instantaneous or sporadic, and the dimensionality of crystal growth.[43-45, 47] The value of n can be either an integer or a half-integer, and each value has been related empirically (and, in some ways, theoretically) to different modes of nucleation and growth that can be correlated with the eventual shapes of the fully formed solids. The value of n is temperature independent as long as the type of the nucleation and growth mechanisms do not change.[48, 49] Using the Avrami model, an acceptable convergence did not occur for the normalized absorbance areas in Figure 1; low R^2 values were found.

The other spectral region of interest for **1** is between 3000 and 3500 cm^{-1} (Figure 2). Three spectral features are evident within this region: 1) the sharp peak at 3300 cm^{-1}, corresponding to the mono-substituted amide in the solid state; 2) the broad peak at 3200 cm^{-1} representing the hydroxyl stretch of the –OH group at position C12; and 3) the weak peak at 3100 cm^{-1}, again corresponding to the mono-substituted amide in the solid state.[42]
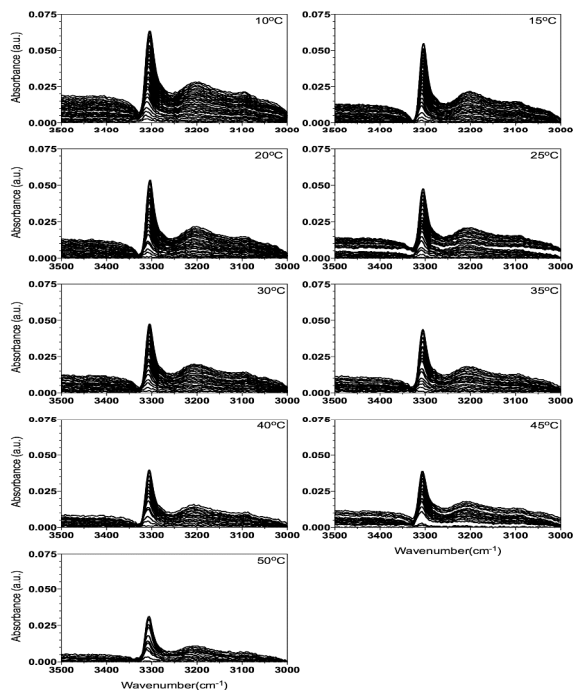
4

Figure 2. Offset FT-IR spectra, using the sol spectra as the baselines, for formation of 2 wt % mineral oil gels of **1** at different temperatures.

Attempts to fit the integrated peak areas of the amide peaks from **1** at 3300 cm^{-1} were unsuccessful: the *n* values varied between 1.23 and 1.91.   This suggests that the specific nature of this N-H bond may not change appreciably during the periods during creation of the gel states being interrogated here. For example, small aggregates from the sol phase may already have established amide bonding interactions. Such a hypothesis is reasonable because this type of intermolecular interaction should have the highest stabilization energy.

For the broad OH-stretching peak[43] at 3200 cm^{-1} and the weak, sharp peak between 3100 and 3200cm^{-1}, the Avrami model fits the data very well (i.e., $R_2 > 0.92$). To begin the fitting, which was done with 1000 iterations, initial values for Y_{max} (equal to 1) and *x* (*x*=0) were defined and *K* and *n* were not provided with initial estimates. The Avrami exponents were fairly consistent for each crystallization temperature (Table 1).

Plots of the data for the peak areas at 3200 and 3100 cm^{-1} yielded the Avrami exponents near to 2 (with the exception of the weak peaks at 3100 cm^{-1} at a crystallization temperature of 50 ^{o}C), indicating either 1-dimensional (i.e., fibrillar) growth and sporadic nucleation or 2-dimensional (i.e., plate-like) growth and instantaneous nucleation.
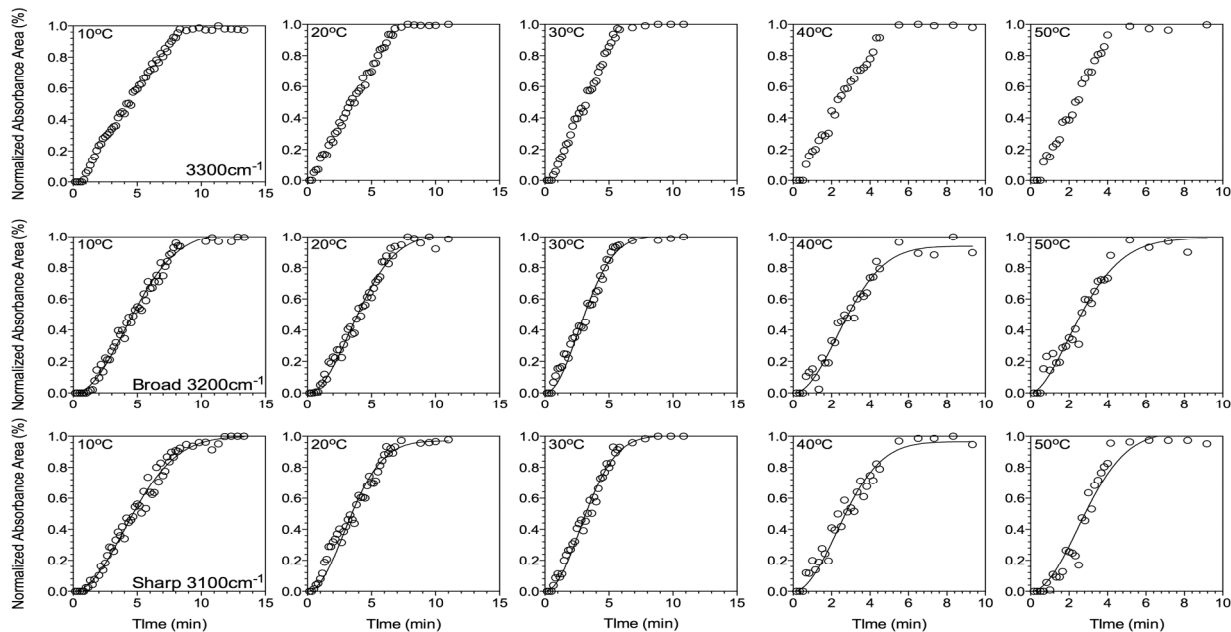
Figure 3. Integrated and normalized data for the areas of the sharp peaks at 3300 cm^{-1} (top row), the broad peaks between 3050 and 3250 cm^{-1} and the weak peaks between 3150 and 3250 cm^{-1} for samples of **1** in the mineral oil at different isothermal crystallization temperatures.

Table 1. Avrami exponents calculated using peak areas at 3300, 3200, and 3100 cm^{-1} at different isothermal crystallization temperatures for sample **1**.

	3300 cm^{-1}		3200 cm^{-1}		3100 cm^{-1}	
T (ºC)	n	R^2	n	R^2	n	R^2
10	1.67	0.99	2.06	0.98	1.95	0.98
15	1.54	0.99	1.76	0.99	1.80	0.98
20	1.59	0.99	1.95	0.98	1.84	0.97
25	1.84	0.94	1.79	0.92	1.82	0.93
30	1.23	0.97	1.89	0.98	1.92	0.98
35	1.74	0.99	1.82	0.97	1.80	0.97
40	1.64	0.76	1.96	0.87	1.86	0.84
45	1.83	0.99	1.91	0.97	1.94	0.96
50	1.91	0.89	1.95	0.95	3.13	0.93

The predictions from the Avrami equation for $n = 2$ can be differentiated by examining the optical micrographs of the fully-formed gel of **1** in mineral oil (Figure 4). Fine fibrous (1D) interconnected structures, which spanthe field of view, are clearly present. On that basis, the mode of nucleation must be sporadic; the alternative, spontaneous nucleation and formation of 2D objects (e.g., platelets), is clearly inconsistent with the structures seen in Figure 4.[43-45]
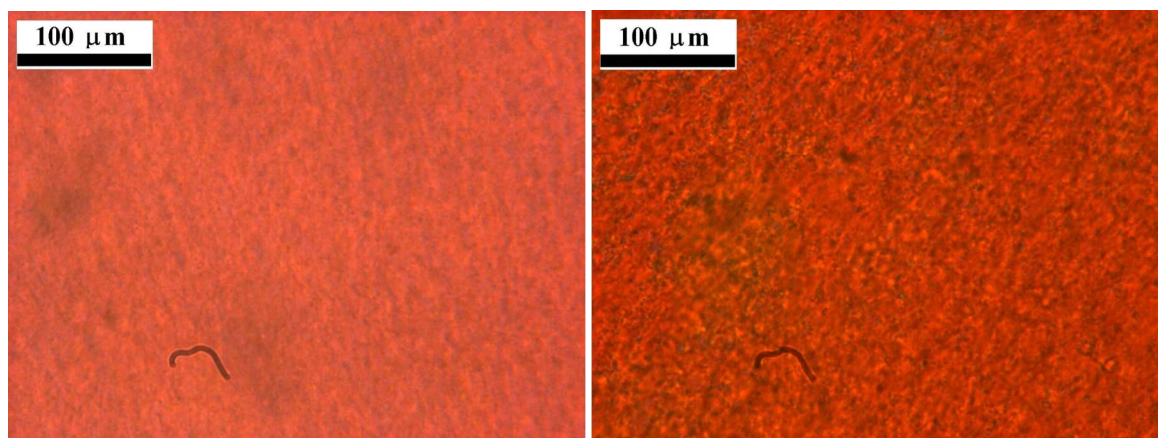
6

Figure 4. Polarizing optical micrographs at 23 °C of a 2 wt % **1** in mineral oil gel prepared by the fast- (left) and slow-cooling (right) protocols .

The same spectral features as found for **1** in Figure 1 are evident at 1375 cm^{-1} for samples of **2** in mineral oil (data not shown). As in the gelation by **1**, this spectral feature is not sensitive to the development of the SAFiN and gelation from the sol state. However, intensities of peaks near 3200 cm^{-1} did change significantly during the phase evolution. In Figure 5, peaks at 3400 and 3300 cm^{-1} correspond to N-H stretching modes of the unsubstituted amide group and the peak at 3200 cm^{-1} corresponds to stretching of the hydroxyl group at C12 of the aliphatic backbone.
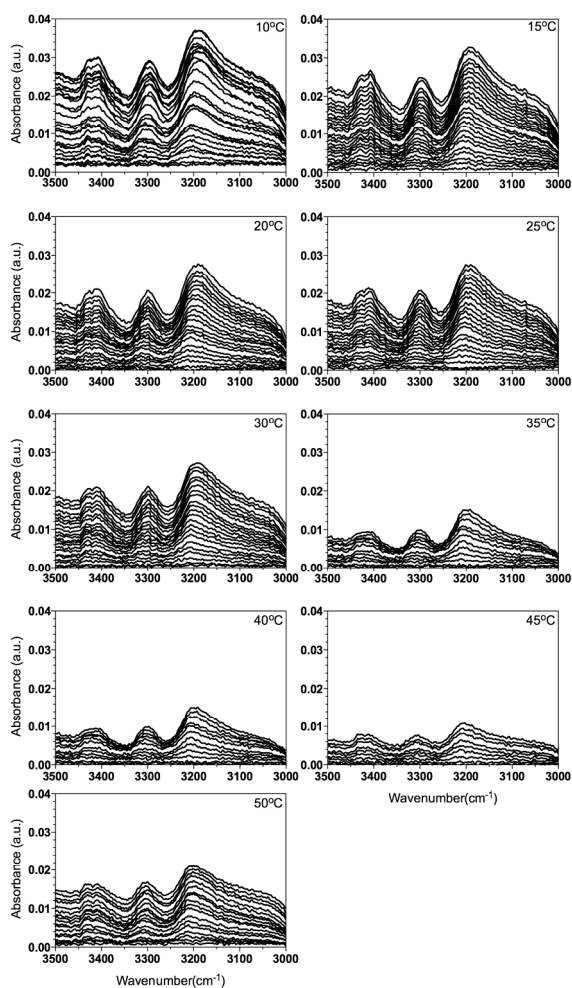
Figure 5. Offset FT-IR spectra, using the sol spectra as the baselines, for formation of mineral oil gels of **2** at different temperatures.

Although the peak intensity changes at 3400 cm^{-1} did not yield reasonable correlations when fitted to the Avrami equation, the amide peak at 3300 cm^{-1} and the hydroxyl peak at 3200 cm^{-1} (d stretch) did (R^2 > 0.94) (Figure 6). Similar confines were placed on the initial parameters to allow the iterative fit to optimize within 1000 iterations. Although all of the data from the peaks at 3400 cm^{-1} do not fit well the Avrami model, those from experiments at low crystallization temperatures (i.e., below 30 $^{\circ}$C) did. This observation suggests the possibility of a two-stage gelation process, as indicated by a small plateau at or near 5 min. We speculate that this change may be associated with a solid-solid transition like that reported for **1** in CCl$_4$.[37] Additional studies in the future will be required to test this hypothesis.
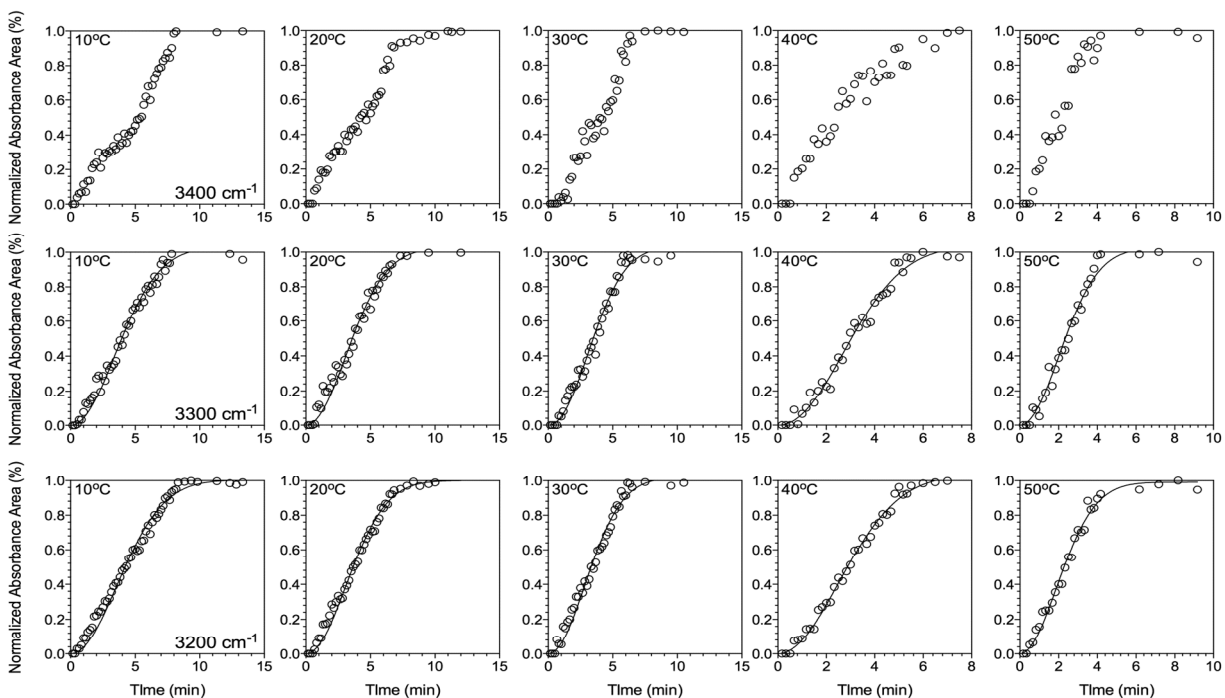

Figure 6. Integrated and normalized data for the peak areas at 3400 cm^{-1} (top row), 3300 cm^{-1} (middle row) and 3200 cm^{-1} (bottom row) for the mineral oil gels of compound 2 at each of the isothermal crystallization temperatures.

The Avrami exponents for the peaks at 3300 and 3200 cm^{-1} were near 2, indicating the possibility of two different nucleation and crystal growth mechanisms (Table 2). POMs again showed a fine structure (Figure 7) that made it difficult to conclude if sporadic or instantaneous nucleation occurred.

Table 2. Avrami exponents from analyses of changes in peak areas at 3400, 3300 and 3200 cm^{-1} for samples of **2** in mineral oil incubated at different temperatures.

	3400 cm^{-1}		3300 cm^{-1}		3200 cm^{-1}	
T ($^{\circ}$C)	*n*	R^2	*n*	R^2	*n*	R^2
10	1.70	0.96	1.85	0.99	1.86	0.99
15	1.40	0.95	1.85	0.99	1.81	0.99
20	1.36	0.85	1.83	0.99	1.82	0.89
25	1.92	0.89	2.10	0.99	1.82	0.95

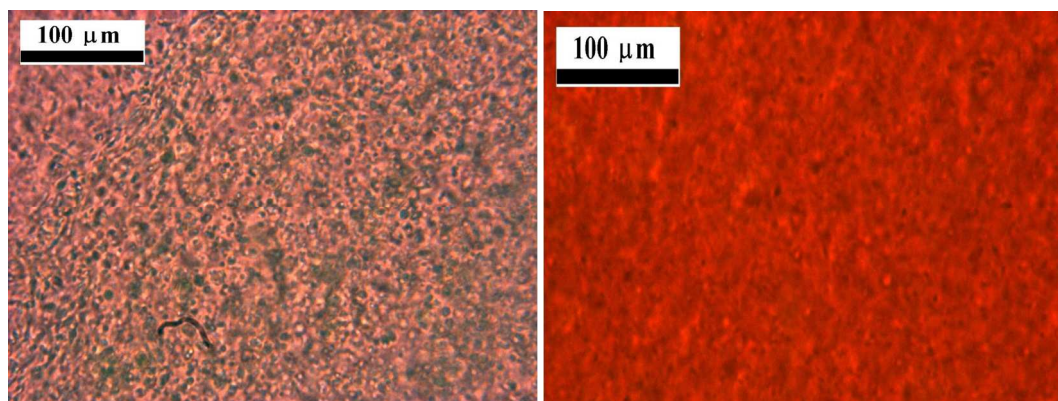| 30		1.90	0.96	2.00	0.98	2.07	0.99
35		1.53	0.97	2.02	0.97	1.84	0.90
40		1.28	0.56	2.07	0.96	1.92	0.92
45		1.67	0.96	1.98	0.96	1.93	0.98
50		1.83	0.96	2.06	0.98	1.96	0.96

Figure 7. Polarizing optical micrograph at 23 ^{o}C of a 2 wt % **2** in mineral oil gel prepared by the fast- (left) and slow-cooling (right) protocols.

If it is assumed that the Avrami exponents *n* are 2 throughout, the corresponding *K* values may be used to determine a global activation energy for crystallization and nucleation using an Arrhenius model (eq. 2)

$$\ln k = \ln A + \frac{E_a}{RT}$$

(2)

where ln *A* is the y-intercept, E_a is the activation energy, *R* is the ideal gas constant and *T* is the crystallization temperature, as before.

The activation energy may only be calculated with the Arrhenius model if the dimensionality of growth, *n*, is the same at each incubation temperature (as is the case here). Thus, the Avrami model was reapplied to each normalized intensity graph while forcing *n* to remain 2. A linear regression between the ln *K* and the inverse of temperature yielded R^2 values greater than 0.85 for all fits (Figure 8A,B).
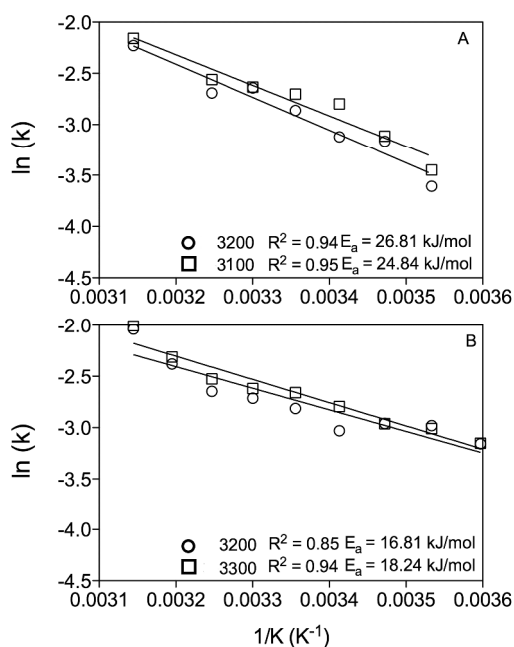
9

Figure 8. Calculation of the activation energy from an Arrhenius plot of the rate constants from the Avrami equation while $n = 2$ for **1** (A) and **2** (B) in mineral oil.

Interestingly, the calculated activation energy for nucleation is lower for **1**, the mono-substituted amide, than that for the unsubstituted amide **2**. This ordering is consistent with the expectation that the activation energy should be lower for the more polar gelator **2** because it should exhibit a greater propensity to undergo phase separation in the low polarity liquid, mineral oil. At this point, given the paucity of activation energies calculated in this fashion, it does not seem appropriate to attempt a detailed interpretation. However, we do note that the magnitudes of the calculated activation energies (inset into Figures 8A and 8B) are what are expected for the formation of H-bonds.

In an attempt to probe further the kinetics of SAFiN formation, Liu's fractal model[22, 26, 29, 31-34, 50-52] was applied using the normalized FT-IR peak intensities and time as the variables. Here X_r represents the normalized FT-IR peak intensity, and in Liu;s model, it is assumed to be a measure of the normalized crystallinity of the system. The method was developed specifically to measure the *in situ* fractal growth of fibrous networks, recognizing that the formation of the fibrous network is controlled by both nucleation and growth.[53] Thus, the Avrami equation was modified to take the form in eq 3:

$$\ln[1 - X_r] = -k^o t^d \tag{3}$$

Here, k^o is a constant related to the rate of nucleation and growth, t is time, and $d = 1, 2,$ or 3 is the Euclidian dimensionality of crystal growth; it may be replaced with the fractal dimension, D_f, if d is a non-integer value.

Analyses of the data indicated that the fractality of the systems (Figure 9) increased unexpectedly with increasing crystallization temperature. As temperature is lowered below T^*, the thermodynamic driving force for phase separation and, thus, the rates of nucleation and growth increase. These factors generally lead to SAFiNs with more branching among the interacting fibers and higher fractal dimensions overall. The opposite trend is predicted by the D_f values obtained here. However, the optical micrographs in Figures 4 and 7 demonstrate that the fractality of these gel networks does not depend acutely on the rate at which their sols are cooled and, in fact, the objects seen are compatible qualitatively with the calculated D_f values.
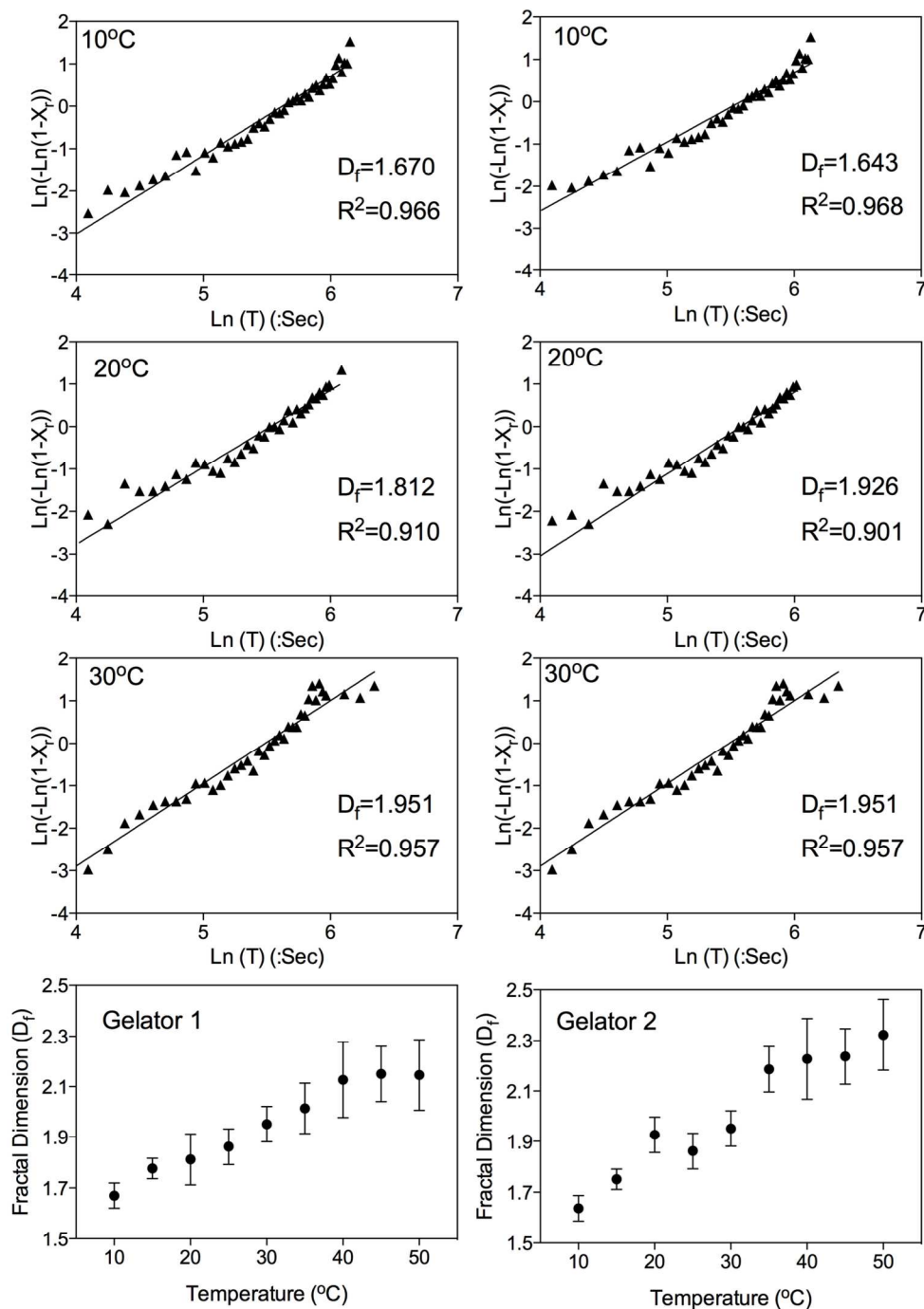
Figure 9. Plots of ln(-ln(1-*Xr*)) versus ln(*T*) to determine the fractal value for gelators **1** (left) and **2** (right) at 10, 20 and 30 °C. Synopses of the fractal values versus crystallization temperature are also shown at the bottom.

Experimental

Materials. Gelators **1** and **2** were available from previous studies.[36] Light mineral oil was from Fisher (Paraffin oil N.F. White, Light, viscosity 125/135) or Sigma-Aldrich (Paraffin oil, white, light, viscosity 14.2 – 17 cst at 40 °C).

Preparation and characterization of gels. A mixture of 2 wt % gelator and mineral oil to form a solution/sol in an oil bath and then placed directly into an ice-water bath for 15 min (fast-cooling method) or were allowed to return very slowly to room temperature at ≤1 $^{\circ}$C/min within the oil bath after heat was removed (slow-cooling method). Polarized optical micrographs (POMs) were recorded on a Leitz 585 SM-LUX-POL microscope equipped with crossed polars, a Leitz 350 heating stage, a Photometrics CCD camera interfaced to a computer, and an Omega HH503 microprocessor thermometer connected to a J-K-T thermocouple. The samples for POM analyses were flame-sealed in 0.4 mm path-length, flattened Pyrex capillary tubes (VitroCom, Inc.), heated to their liquid phase, and cooled according to the fast-cooling protocol. Images were recorded with a full-wave plate. Differential scanning calorimetry (DSC) was performed on a TA 2910 differential scanning calorimeter interfaced to a TA Thermal Analyst 3100 controller under a slow stream of nitrogen flowing through the cell. Rheological measurements were obtained at 25 $^{\circ}$C on an Anton Paar Physica MCR 301 strain-controlled rheometer using a Peltier temperature-controller and parallel plates (25 mm diameter). The gap between the plates was 0.5 mm and the data were collected using Rheoplus/32 Service V3.10 software. Before recording data, each sample was placed between the plates of the rheometer and heated to 125 $^{\circ}$C to ensure that a solution/sol was present. It was cooled to 25 $^{\circ}$C (~20 $^{\circ}$C/min) and incubated there for 30 min to reform the gel.

Protocols for FT-IR kinetic measurements. Fourier transform infrared spectroscopy (FTIR) mapping experiments were conducted on the endstation of the mid-IR beamline (01B1-01, Canadian Light Source, Saskatoon, SK). Gels were prepared at 2 wt % of **1** or **2** in mineral oil by heating the mixture to 120 $^{\circ}$C for 20 min to prepare a sol state. A drop of sol was placed between two pre-heated 2 mm thick, 25 mm diameter CaF_2 disks separated by a 15 μm Teflon spacer. The samples between the CaF_2 disks were then placed into a temperature controlled peltier stage (Linkham, Surry, UK) that was set at crystallization temperatures ranging from 5 $^{\circ}$C to 40 $^{\circ}$C in 5 $^{\circ}$C increments. Under a dry nitrogen atmosphere, the samples and stage were placed onto the XY mapping stage of a Bruker vertex 70v FT-IR coupled to a Bruker Hyperion 3000 FPA microscope (Bruker Optics Inc., Milton, ON, Canada). The radiation was focused on the sample using a 36x magnification Schwarzschild condenser, and collected by a 36x magnification Schwarzschild condenser. The spectra were acquired at a resolution of 4 cm^{-1} using 512 co-additions. Single channel traces were obtained using the fast Fourier transform algorithm, without any zero-filling, after applying a Blackman-Harris 3-Term apodization function. For single spectra, measurements of reference single channel traces were carried out in the sol state. Spectra were collected every 10 s—individual spectra required 7 s to record; a 3 s delay was imposed before recording the next spectrum--until the sample temperature reached the crystallization temperature and then for an additional 5 min at the crystallization temperature. The total measurement periods were 10--15 min. For purposes of clarity, only every other spectrum is shown in Figures 1, 2, and 5 above.

Conclusions

In many cases, the rapidity of the processes leading to the transformation of sols to gels makes it difficult to view the intervening events in real time. The results presented here demonstrate the utility of employing fast infrared spectroscopic methods to follow changes in the environments of individual functional groups as gelator molecules aggregate and form SAFiNs. The conclusions reached from analyses of the results for formation of **1** and **2** are intriguing, but they may or may not be general. Also, if the gelator structures are more complex than those of **1** and **2**, false conclusions may be reached if one group's interactions influence the local environments and, thus, the interactions of other groups in the vicinity. Clearly, the results found in this study, with two gelators of similar structure, lead to as many questions as answers. Regardless, the observations demonstrate the utility of fast infrared spectroscopy as a valuable new tool to delve into the detailed mechanisms of self-assembly. Future experiments can capitalize on what has been learned here to provide the answers to many of the outstanding questions, for example, by examining the kinetics of aggregation of a homologous series of amides structurally related to **1** and **2**. Perhaps more importantly, this technique is amenable to use with a wide range of other gelator systems. Finally, by understanding the activation energies as a function of molecular structure, we may be able to tailor the gelation ability of new classes of poorly understood gelators and design others.

References.

1. P. Jonkheijm, P. van der Schoot, A. P. H. J. Schenning and E. W. Meijer, *Science*, 2006, **313**, 80-83.
2. R. Weiss, G., *Journal of the American Chemcial Society*, 2014.
3. J. H. van Esch, *Langmuir*, 2008, **25**, 8392-8394.
4. D. Li and Y. N. Xia, *Nano Lett.*, 2004, **4**, 933-938.
5. K. Hanabusa, T. Miki, Y. Taguchi, T. Koyama and H. Shirai, *J. Chem. Soc.-Chem. Commun.*, 1993, 1382-1384.
6. J. Jin, M. Song and F. Pan, *Thermochim. Acta*, 2007, **456**, 25-31.
7. D. Dasgupta, S. Srinivasan, C. Rochas, A. Ajayaghosh and J.-M. Guenet, *Soft Matter*, 2011, **7**, 9311-9315.
8. W. Edwards, C. A. Lagadec and D. K. Smith, *Soft Matter*, 2011, **7**, 110-117.
9. J. Gao, S. Wu, Emge. T. and M. A. Rogers, *Crystal Engineering Communications*, 2013, **15**, 4507-4515.
10. A. R. Hirst and D. K. Smith, *Langmuir*, 2004, **20**, 10851-10857.
11. Y. Jeong, K. Hanabusa, H. Masunaga, I. Akiba, K. Miyoshi, S. Sakurai and K. Sakurai, *Langmuir*, 2005, **21**, 586-594.
12. S. Wu, J. Gao, Emge. T. and M. A. Rogers, *Crystal Growth & Design*, 2013, **13**, 1360-1366.
13. S. Wu, J. Gao, Emge. T. and M. A. Rogers, *Soft Matter*, 2013, **9**, 5942-5950.
14. N. Yan, Z. Xu, K. K. Diehn, S. R. Raghavan, Y. Fang and R. G. Weiss, *Langmuir*, 2013, **29**, 793-805.
15. M. A. Rogers and R. G. Weiss, *New Journal of Chemistry*, 2015.
16. L. Chen, M. G. Corradini and M. A. Rogers, *Colloid & Polymer Science*, 2015.
17. M. A. Rogers, S. Abraham, F. Bodondics and R. G. Weiss, *Crystal Growth & Design*, 2012, **12**, 5497-5504.
18. S. Abraham, Y. Lan, R. S. H. Lam, D. A. S. Grahame, J. J. H. Kim, R. G. Weiss and M. A. Rogers, *Langmuir*, 2012, **28**, 4955-4964.
19. M. A. Rogers and A. G. Marangoni, *Langmuir*, 2009, **25**, 8556-8566.
20. K. K. Diehn, H. Oh, R. Hashemipour, R. G. Weiss and S. R. Raghavan, *Soft Matter*, 2014, **10**, 2632-2640.
21. K. K. Diehn, H. Oh, R. Hashemipour, R. G. Weiss and S. R. Raghavan, *Soft Matter*, 2014, **10**, 2632-2640.
22. R. Y. Wang, P. Wang, J. L. Li, B. Yuan, Y. Liu, L. Li and X. Y. Liu, *Physical chemistry chemical physics : PCCP*, 2013, **15**, 3313-3319.
23. W.-C. Lai and J.-P. Liao, *Materials Chemistry and Physics*, 2013, **139**, 161-168.
24. M. A. Rogers, S. Abraham, F. Bodondics and R. G. Weiss, *Crystal Growth & Design*, 2012, **12**, 5497-5504.
25. D. L. VanderHart, J. F. Douglas, S. D. Hudson, J. M. Antonucci and E. A. Wilder, *Langmuir*, 2011, **27**, 1745-1757.
26. X. Y. Liu and P. D. Sawant, *Applied Physics Letters*, 2001, **19**, 3518-3520.
27. P. Terech, *Journal of Colloid and Interface Science*, 1985, **107**, 244-255.
28. R. S. H. Lam and M. A. Rogers, *Crystal Engineering Communications* 2010, **13**, 866-875.

29.   J. L. Li, R. Y. Wang, X. Y. Liu and H. H. Pan, *Journal of Physical Chemistry B*, 2009, **113**, 5011-5015.
30.   J. W. P. Schmelzer, in *Molecular Gels: Materials with Self-Assembled Fibrillar Networks*, eds. R. G. Weiss and P. Terech, Springer, Dordrecht, The Netherlands, 2006.
31.   J.-L. Li, B. Yuan, X.-Y. Liu, X.-G. Wang and R.-Y. Wang, *Crystal Growth & Design*, 2011, **11**, 3227-3234.
32.   R. Y. Wang, X. Y. Liu, J. Narayanan, J. X. Xiong and J. L. Li, *Journal of Physical Chemistry B*, 2006, **10**, 25797-25802.
33.   J. L. Li, X. Y. Liu, R. Y. Wang and J. Y. Xiong, *Journal of Physical Chemistry B*, 2005, **109**, 24231-24235.
34.   X. Y. Liu and P. D. Sawant, *CHEMPHYSCHEM*, 2002, **4**, 374-377.
35.   M. Suzuki, Y. Nakajima, M. Yumoto, M. Kimura, H. Shirai and K. Hanabusa, *Langmuir*, 2003, **19**, 8622-8624.
36.   V. A. Mallia, M. George, D. L. Blair and R. G. Weiss, *Langmuir*, 2009, **25**, 8615-8625.
37.   V. A. Mallia, P. D. Butler, B. Sarkar, K. T. Holman and R. G. Weiss, *Journal of the American Chemical Society*, 2011, **133**, 15045-15054.
38.   R. S. H. Lam and M. A. Rogers, *Crystal Growth & Design*, 2011, **11**, 3593-3599.
39.   R. Lam, L. Quaroni, T. Pederson and M. A. Rogers, *Soft Matter*, 2010, **6**, 404-408.
40.   M. A. Rogers, A. Bot, R. Lam, S.H., T. Pedersen and T. May, *Journal of Physical Chemistry*, 2010, **114**, 8278-8295.
41.   X. Huang, P. Terech, S. R. Raghavan and R. G. Weiss, *Journal of the American Chemical Society*, 2005, **127**, 4336-4344.
42.   D. Lin-Vien, N. B. Colthup, W. G. Fateley and J. G. Grasselli, *The Handbook of Infrared and Raman Characteristic Frequencies of Organic Molecules*, Academic Press, London, UK, 1991.
43.   M. Avrami, *Journal of Chemical Physics*, 1939, **7**, 1103-1112.
44.   M. Avrami, *Journal of Chemical Physics*, 1940, **8**, 212-226.
45.   M. Avrami, *Journal of Chemical Physics*, 1941, **9**, 177-184.
46.   M. A. Rogers and A. G. Marangoni, *Crystal Growth & Design*, 2008, **8**, 4596-4601.
47.   A. G. Marangoni, in *Fat Crystal Networks*, ed. A. G. Marangoni, Marcel Dekker, New York, 2005, pp. 21-82.
48.   B. Wunderlich, *Macromolecular Physics*, Academic Press, New York, NY, 1976, p 385.
49.   J. M. Schultz, *Polymer Materials Science*, Prentice Hall, Englewood Cliffs, New Jersey, 1974, Vol 2, pp16-52.
50.   S. Liu, W. Yu and C. Zhou, *Soft Matter*, 2013, **9**, 864-874.
51.   X. Y. Liu and P. D. Sawant, *Advanced Materials*, 2002, **14**, 421-426.
52.   B. Yuan, J.-L. Li, X. Y. Liu, Y.-Q. Ma and Y. J. Wang, *Soft Matter*, 2012, **8**, 5187-5193.
53.   X. Y. Liu, *Topics in Current Chemistry*, 2005, **256**, 1-37.
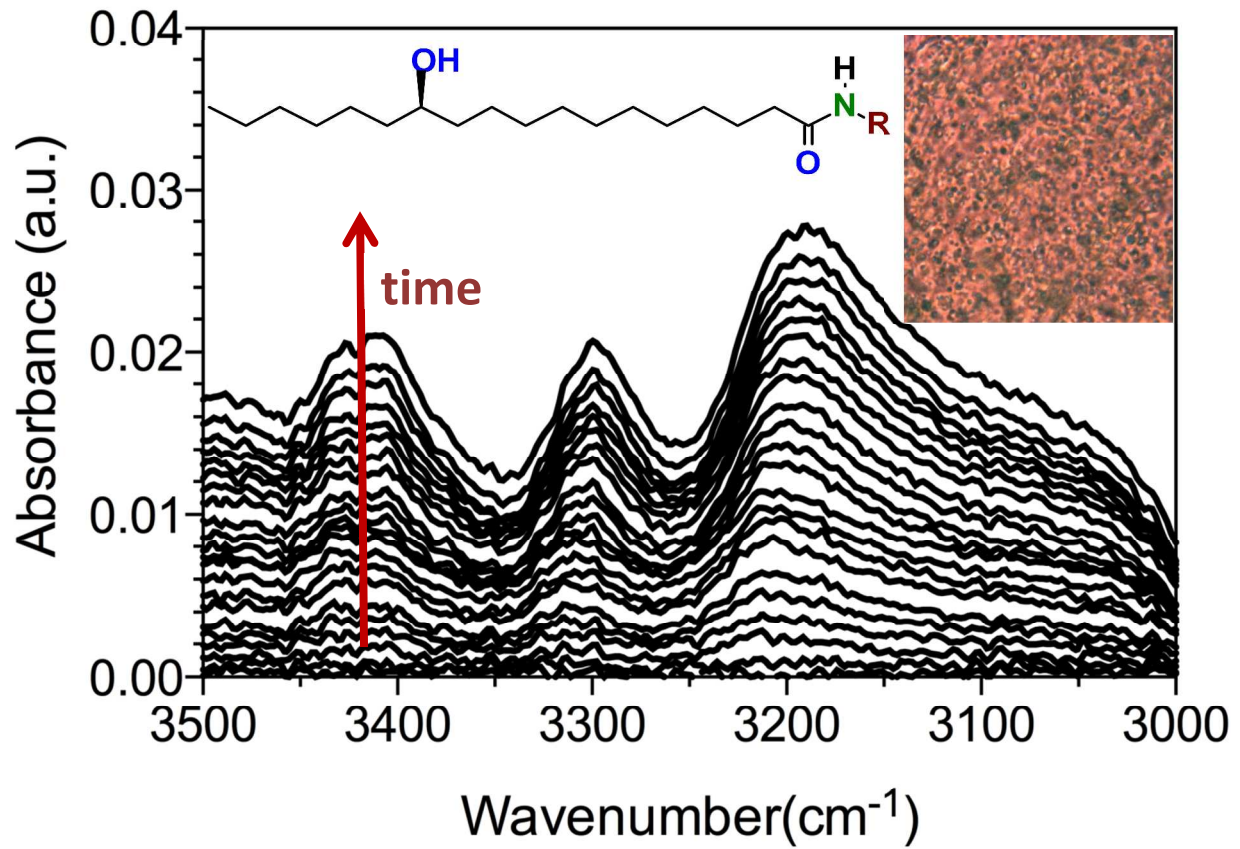
Infra-red synchrotron radiation is used to monitor the formation of fibrillar networks as sols of simple gelators become gels.